THE JOURNAL OF PHYSICAL CHEMISTRY C

Article

pubs.acs.org/JPCC

Thermo-Active Behavior of Ethylene-Vinyl Acetate | Multiwall Carbon Nanotube Composites Examined by in Situ near-Edge X-ray Absorption Fine-Structure Spectroscopy

A. Douglas Winter,[†] Eduardo Larios,[‡] Faisal M. Alamgir,[§] Cherno Jaye,[∥] Daniel A. Fischer,[∥] Mária Omastová,[⊥] and Eva M. Campo*[,†,‡]

[†]School of Electronic Engineering, Bangor University, Bangor LL57 1UT, United Kingdom

[‡]Department of Physics and Astronomy, University of Texas at San Antonio, San Antonio, Texas 78249, United States

[§]School of Materials Science & Engineering, Georgia Institute of Technology, Atlanta, Georgia 30332, United States

[∥]Material Measurement Laboratory, National Institute of Standards and Technology, Gaithersburg, Maryland 20899, United States

[⊥]Polymer Institute, Slovak Academy of Sciences, Bratislava 84541, Slovak Republic

ABSTRACT: NEXAFS spectroscopy was used to investigate the temperature dependence of thermally active ethylene-vinyl acetate | multiwall carbon nanotube (EVA|MWCNT) films. The data shows systematic variations of intensities with increasing temperature. Molecular orbital assignment of interplaying intensities identified the 1s → $\pi^*_{C=C}$ and 1s → $\pi^*_{C=O}$ transitions as the main actors during temperature variation. Furthermore, enhanced near-edge interplay was observed in prestrained composites. Because macroscopic observations confirmed enhanced thermal-mechanical actuation in prestrained composites, our findings suggest that the interplay of C═C and C═O π orbitals may be instrumental to actuation.

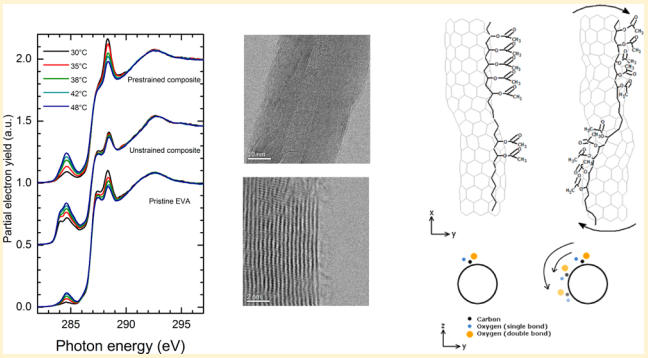

1. INTRODUCTION

High molecular integration afforded by conveniently processed soft-matter assemblies paves the way toward mechanically responsive systems whose extreme structure−property complexity closely resembles paradigms observed in nature.[1−4] This resemblance has fueled the investigation of smart systems in the context of artificial muscles and biomedical implants as well as textiles and nanopositioners among others.[2] In this scenario, not only can mechanical responses and shape memory effects be programmed within native molecular structures of polymers, upon adequate processing, but also they can be suitably combined with additional functionalities such as permeability, dielectricity, or optical transparency.[2]

The wealthy synthesis-property space portrayed by mechanically responsive systems is further enhanced by the addition of fillers. Indeed, the inherent molecular architecture flexibility in polymers allows filler addition, which can, in turn, also feature functionalities of their own. This is the case of carbon nanotubes (CNTs),[5] with remarkable properties inclusive of mechanical actuation in ionic solutions[1,6] and upon suitable bonding within polymeric matrices.[2] Synthesis/property relations are currently the subject of much study in the context of structural[7] and active applications, which extend across the materials space from liquid-crystal elastomers[8−10] to CNTs and graphene polymer composites.[11−13] Finally, the application space associated with mechanically responsive systems is also augmented by the possibility of multiple stimuli suited to trigger actuation,[3] inclusive of electrical,[14] thermal, and optical,[10,13,15] promising engineering flexibility toward device design.

Expectation toward deployment of smart devices based on smart composites is mostly hindered by a lack of understanding of the underlying mechanisms.[16] Filler dispersion and alignment are often cited as necessary conditions for effective or enhanced actuation.[12,17] Precisely, one of the greater challenges in the fabrication of active polymer nanocomposites is filler dispersion, commonly attempted through sonication processes[18] or by addition of chemical dispersants.[17] In addition, straining procedures have been designed to promote carbon nanotube alignment, possibly leading to mechanical-energy storage, in a variety of polymeric composites.[12,19]

Recently, a photothermal mechanical response has been observed in ethylene vinyl-acetate nanocomposites.[17] EVA is a low-cost polymer that has found a wide range of structural applications and has been successfully used as a reversible shape-memory polymer (SMP).[20] Large mechanical responses were favored by the addition of MWCNT fillers to EVA, amenable to enhanced light absorption and thermal capacity,

Received: September 20, 2013
Revised: January 25, 2014
Published: January 27, 2014

yielding strains on the order of 1−15%, with sharp onset responses, and relaxation times on the order of tens of seconds. Intriguingly, shape-memory polymers and composites containing elastomeric matrix with carbon nanotubes can either contract or expand upon stimulation, depending on prestrain.[15,19] The extent of prestrain bears important consequences in these material systems, and the mechanism responsible for the bimodal behavior (contraction or expansion) with the applied prestrain is not understood at present.[19] Indeed, bimodal and reversible actuation of MWNT/elastomer nanocomposites induced by infrared irradiation was first reported in PDMS|MWCNT composites.[15] In this scheme, reversible expansion occurs at small prestrains and reversible contraction at large prestrains. The contracting scenario has been modeled as light being rapidly absorbed by CNTs, producing a thermal perturbation to the surrounding polymeric chains, affecting the prestrained distribution. Polymeric chains could then relax and contract, resulting in mechanical output. The expanding scenario is still a matter of much debate.

Overall, a fundamental understanding of photothermal actuation down to the molecular level is still missing, and the proposed models are yet to be verified through direct experimental data. In particular, the molecular conformation between CNTs and polymer chains is the subject of much discussion in nanocomposites, offering insights into physical adsorption mechanisms,[21] conformational configurations,[22] and nucleation dynamics.[23] However, details of molecular conformation in smart composites have not been explored to the best of our knowledge.

In this study, the thermo-active behavior of EVA | MWCNT composites was examined by in situ near-edge X-ray absorption fine-structure (NEXAFS) spectroscopy.[24,25] Nanocomposites described in this article, with prestrains on the order of 50%, belong to the contractive bimodal response scenario.[26] In this scheme, photothermo-mechanical actuation is promoted by CNT's photon−phonon coupling, where thermal energy is released to surrounding polymeric chains. NEXAFS has proved to be an invaluable tool in the study of polymers and CNTs, providing a wealth of information from alignment of polymer chains[24] and CNTs[27] to surface functional groups on CNTs and bond hybridization.[28]

The beamline of choice for these experiments was the National Institute of Standards and Technology (NIST) U7A beamline at the National Synchrotron Light Source (NSLS) at Brookhaven National Laboratory (BNL). The U7A beamline is well-suited for the study of soft matter. In addition, it is uniquely equipped for in situ experiments, with loading chambers readily available for thermal, electrical, and optical in situ measurements. The goal of this approach was to use NEXAS for the exploration of mechanisms behind thermal actuation by probing into the fine structure of EVA|CNT composites. It is worth emphasizing that clarification on the nature of filler−matrix bonding in the structural and smart composites will be of paramount importance to both communities given the scarcity of NEXAFS interfacial studies in polymer nanocomposites.[29−31] To our knowledge, this is the first attempt to measure fine electronic structure in the context of smart composites.

2. EXPERIMENTAL METHODS

2.1. Materials. Commercial ethylene vinyl acetate copolymer EVA (Evatane 28-25, Arkema, France) containing 28 wt % of vinyl acetate and chloroform ($CHCl_3$ p.a., Mikrochem, Slovakia) were used as matrix and solvent, respectively. Reported values for T_g and T_m are −28 and 83 °C, respectively.[32] Nanofillers were MWCNT (Nanostructured & Amorphous Materials, Inc.; Houston, TX). The purity of MWCNT exceeds 95 wt %, the outside diameter distribution is between 60 and 100 nm, the CNT lengths are between 5 and 15 μm, and the surface area is 64 m^2/g. Cholesteryl 1-pyrenecarboxylate (PyChol) was used as a compatibilizer, and synthesis details are provided elsewhere.[17]

2.2. Nanocomposite Preparation. Following previously reported procedures,[17] a MWCNT/PyChol weight ratio of 1:5 was used (0.7 wt %; 70 mg MWCNTs and 350 mg of cholesteryl pyrenecarboxylate (PyChol)). Upon dispersion in 100 mL of chloroform, the solution was sonicated for 1 h under magnetic stirring with a Hielscher 400 S sonicator at an amplitude of 20% (~35 μm, ~60 W/cm^2) and a duty cycle of 100%. Figure 1a shows the molecular structrue of EVA. The

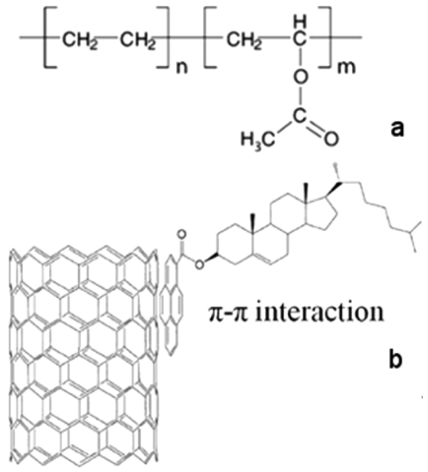

Figure 1. Schematic featuring molecular structures of (a) EVA and (b) proposed MWCNT | PyChol interaction.

noncovalent modification of MWCNTs implies the promotion of $\pi-\pi$ interactions between pyrene groups and graphitic walls of MWCNTs. Cholesteryl groups were designed to prevent $\pi-\pi$ interactions among adjacent MWCNTs, avoiding agglomeration and assisting dispersion.

Upon sonication, 10 g of EVA (Evatane 28-25) was added, and the final solution was magnetically stirred for several hours. The solution was subsequently poured into a Teflon-coated Petri dish and dried at laboratory temperature for 12 h prior to gradual oven drying at 40, 60, and 70 °C for several hours. Finally, composites were placed in a vacuum oven for 6 h at 70 °C. Composite films were then compression-molded in a laboratory press (Fontijne SRA-100, The Netherlands) for 15 min under a pressure of 2.4 MPa and a temperature of 80 °C. The pressed composite samples were strained up to 50% at 50 °C for 20 min using a custom-made stretching apparatus. Subsequently, the stretched samples were cooled in ice water to fix the orientation of CNTs. Two EVA|MWCNT (0.7 wt %) were prepared following this procedure: one with no prestrain and one with 50% prestrain. Pristine PyChol, EVA, and methanol-dispersed CNTs were also used for comparison.

2.3. Aberration-Corrected TEM Analysis and Polarized Raman Spectroscopy. Untreated MWCNTs were characterized using a JEOL JEM-2010F field-emission operated at 200 kV and a JEOL JEM-ARM200F electron microscope. STEM

dx.doi.org/10.1021/jp409413k | J. Phys. Chem. C 2014, 118, 3733−3741

images were simultaneously recorded in both the high-angle anular dark-field (HAADF) and bright-field (BF) modes at 80 kV. Probe correction was performed with a CEOS corrector obtaining a 12-fold Ronchigram with a flat area of ~40 mrad. Images were registered with a condenser lens aperture of 30 μm (convergence angle 25 mrad), and the HAADF collection angle ranged from 45 to 180 mrad. The spot size used was ~35 pA.

Polarized Raman spectroscopy was conducted on a 161B Renishaw system equipped with a 632 He−Ne laser for the purpose of addressing nanofillers alignment upon processing.

2.4. Near-Edge X-ray Absorption Fine-Structure Spectroscopy. Near-edge X-ray absorption fine-structure spectroscopy probes transitions of excited 1s core electrons to unoccupied (bound or continuum) states, emitting a photoelectron. Upon core−hole decay, released energy promotes two processes: fluorescence emission (bulk sensitive) or Auger electron emission (surface sensitive, partial electron yield mode), as seen in Figure 2. On observing these processes,

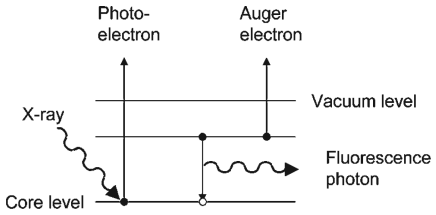

Figure 2. Schematic of underlying processes in NEXAFS.

information on the electronic structure, chemical environment, and orientation of molecules is derived.[33] When compared with other techniques, such as infrared spectroscopy (IR), NEXAFS places fewer demands on the physical characteristics of substrates (such as transparency), which is advantageous for in situ analysis. It also provides high sensitivity upon chemical changes.[34]

Carbon K-edge spectra were collected at U7A (NSLS-BNL) in partial electron yield (PEY) mode using a horizontally polarized beam. A toroidal spherical grating monochromator with 600 lines/mm and slits opening of 30 μm × 30 μm provided an energy resolution of ~0.1 eV at the carbon edge. An electron floodgun set at 60 μA was used to mitigate surface charging. The resulting beam size is 2 mm × 2 mm, and given the chemistry of the composite, we find that 1.5 in a million monomeric units are vinyl acetate groups in proximity to the MWCNT, which add up to 3 × 10^8 vinyl acetate groups surrounding CNTs within the sampled volume.

For in situ temperature studies, samples were secured with a vacuum-safe epoxy (Torr-Seal) on a tantalum metal plate that was inserted on a customized heating stage. The stage angle was controlled by a goniometer, and the temperature was controlled by a voltage supply. Temperature oscillations were observed as ±1.5 °C of the set point. Genzer and co-workers published more exhaustive details on the in situ capabilities of the beamline.[35] The prestrained composite was mounted with the strain direction perpendicular to the beam polarization. Spectra were acquired at magic angle by sequentially running macros that controlled the coordinates of the stage and specified the energy parameters. The temperature sequence was 30, 35, 38, 42, and 48 °C.

The PEY signals were normalized to the incident beam intensity using the photoemission signal from a freshly evaporated Au mesh located along the incident beam path. The spectra were energy-calibrated using the photoemission current from an amourphous carbon mesh also located along the path of the incident beam. Spectra were calibrated and normalized using standard routines from the Athena software.[36]

3. RESULTS AND DISCUSSION

3.1. Room Temperature NEXAFS Spectra. The NEXAFS spectrum of pristine EVA (Figure 3) presents three prominent

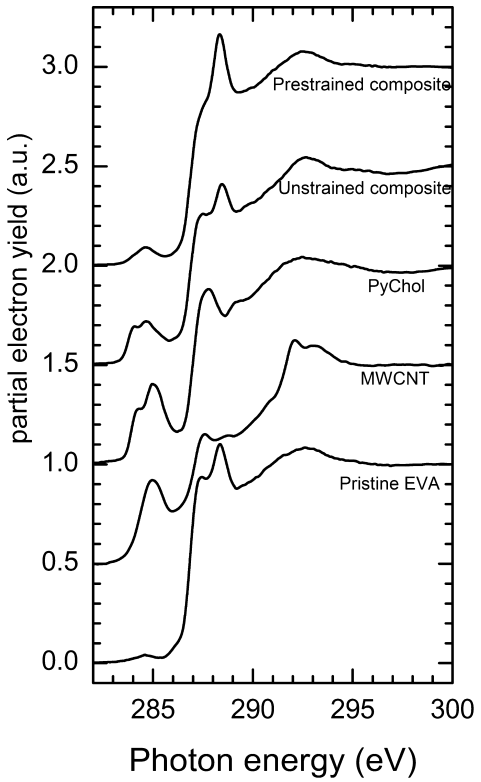

Figure 3. Carbon K-edge NEXAFS spectra acquired at magic angle and room temperature of (bottom to top) pristine EVA, PyChol, EVA/0.7 wt % MWCNT composite, and prestrained EVA/0.7 wt % MWCNT composite.

features with an additional low-intensity feature at 284.5 eV, indicative of C=C groups. This is taken to be contamination, as no such group exists in pristine EVA. The emission at 287.5 eV is assigned to 1s → σ^*_{C-H}, 288.4 eV corresponds to 1s → $\pi^*_{C=O}$ from vinyl acetate, and the broader resonance at 292.4 eV arises from 1s → σ^*_{C-C}.

The NEXAFS spectrum of MWCNTs shows prominent emissions at 285, 287.6, and 292 eV, attributed to C=C π^*, C−H σ^*, and C−C σ^*, respectively, with C=O π^* and C−O σ^* in the range of 288 to 289 eV.[37] The CNT spectra are in good agreement with reported spectra of unpurified MWCNTs,[27] showing C=O π^*, possibly associated with native defects along graphitic walls,[38] as well as an unexpectedly large contribution to the C−H σ^* and C−O σ^* emissions, similar to those reported in ozone-treated CNTs.[28] The possibility of residual species on untreated CNTs was investigated by STEM (Figure 4).

Low-magnification STEM images show undulated external layers of CNTs (Figure 4, left). This pattern transfers throughout at least a few graphitic layers through the inner tube, suggesting structural defects. Local high crystallinity of graphitic walls (middle section in Figure 4, right) coexists with

dx.doi.org/10.1021/jp409413k | J. Phys. Chem. C 2014, 118, 3733−3741

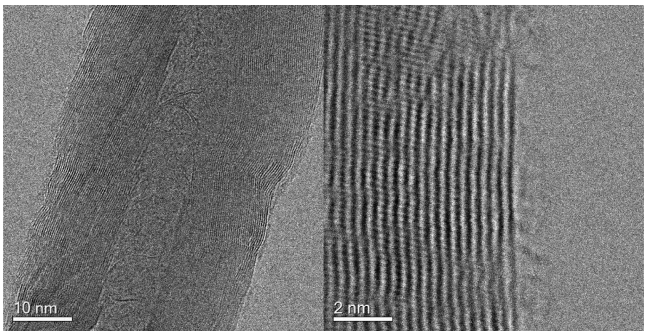

Figure 4. Low-magnification STEM image showing uneven external graphitic layers of MWCNTs with bends along the wall (left) and residual species at higher magnification (right).

structural defects, as seen in the upper left region in Figure 4, right. The sharp atomic contrast is convoluted by the presence of an uneven layer that we tentatively attribute to residual species as discussed above. Recently, in situ aberration-corrected TEM studies explored chemistry dynamics during CNT oxidation, where a similar carbonaceous layer has been identified.[39]

Similar features to EVA are observed in the PyChol NEXAFS spectrum (Figure 3) given the similar chemical species in both PyChol and EVA. The 1s → $\pi^*_{C=C}$ transitions are responsible for the peaks at 284.2 and 285 eV. The different energies are indicative of different chemical environments for C═C groups. The 1s → σ^*_{C-H} transitions are present at 287.7 eV, and at 289.1 eV, emissions are observed from the 1s → $\pi^*_{C=O}$ transitions, which are less intense that in EVA because there is only one C═O group per PyChol molecule.

Intensities associated with the 1s → σ^*_{C-H}, 1s → $\pi^*_{C=O}$, and 1s → σ^*_{C-C} transitions are present in the unstrained composite (Figure 3) at the same photon energies and with similar intensities as in pristine EVA. Transitions 1s → $\pi^*_{C=C}$ of sp^2-hybridized carbon atoms in nanotubes appear at 284.7 eV. At slightly lower energies, the 1s → $\pi^*_{C=C}$ transitions from PyChol can be observed (284.1 eV). The main contributor to the 1s → $\pi^*_{C=O}$ transitions is EVA, whereas PyChol and CNTs dominate the 1s → $\pi^*_{C=C}$ transitions. All of the components contribute to the 1s → σ^*_{C-H} and 1s → σ^*_{C-C} transitions. The dual functionality of the PyChol structure is conducive to the dispersion of CNTs (prevented through the action of cholesteryl groups) and to the bonding of EVA polymers to CNTs. Indeed, pyrene groups in PyChol molecules attached to graphitic walls through $\pi-\pi$ interactions provide a similar environment to pristine CNTs for EVA molecules to bond.

Remarkably, upon stretching, transitions from the pre-strained composite produce a significantly different spectrum (Figure 3). The intensity at 288.4 eV from C═O groups shows a 50% increase, causing the 287.7 eV feature to appear as a shoulder. Straining is likely to promote alignment of polymer chains, conferring a preferred distribution of the C═O groups.[24] The distinct double 1s → $\pi^*_{C=C}$ transitions observed prior to stretching now appear convoluted as one feature. This emission shows a reduced intensity when compared to the unstrained composite. We hypothesize that straining has promoted alignment of CNTs, yielding a higher amount of π^* vectors (normal to the CNT surface) parallel to the incoming electric field (whose polarization is parallel to the CNT surface). The resulting overlap between the polarized electric field and the π system is decreased owing to the orbital geometry of the π system, thus diminishing the 1s → $\pi^*_{C=C}$ intensity observed by NEXAFS.

By conducting polarized Raman spectroscopy along the main axis orientation before and after strain, an indication of achieved alignment can be provided.[40] Indeed, monitoring of D and G band intensities from CNTs in a matrix whose straining direction is oriented parallel (∥) and perpendicular (⊥) to the laser polarization is commonly performed to address the degree of filler alignment upon straining. Figure 5 shows

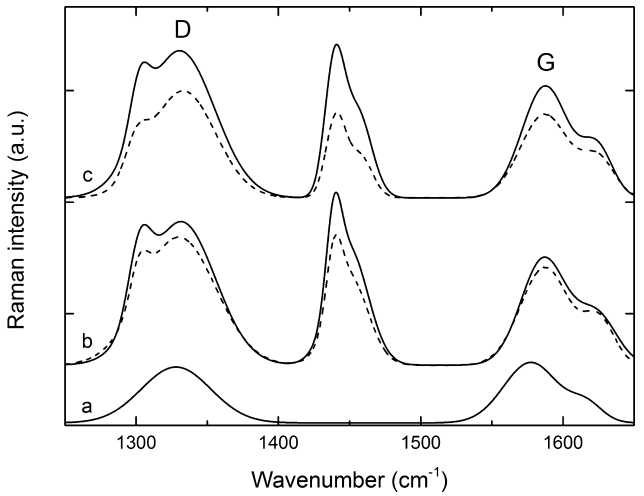

Figure 5. Raman spectrum from drop-casted MWCNTs on Si (a). Polarized Raman spectra acquired at parallel (solid line) and perpendicular (dashed line) configurations, as discussed in the text, from unstrained (b) and strained (c) EVA|MWCNT composites.

Raman spectra from pristine drop-casted MWCNTs as well as unstrained and strained EVA|MWCNT composites. Spectra from composites were acquired along parallel and perpendicular orientations, with D and G bands at 1336 and 1585 cm^{-1} originating from MWCNTs, as seen in Figure 5a, and commonly attributed to disorder and graphitic crystallinity in CNTs, respectively.[41] Additional emissions are observed in spectra from composites at 1302 and 1439 cm^{-1}, which have been attributed to CH_2 twisting and scissoring vibrational modes on EVA.[42]

Ratios of $ID_{\parallel}/ID_{\perp}$ and $IG_{\parallel}/IG_{\perp}$ were both 1.1 in unstrained composites, suggesting isotropy. However, upon straining, $ID_{\parallel}/ID_{\perp}$ and $IG_{\parallel}/IG_{\perp}$ were 1.37 and 1.34, respectively. This degree of gained alignment upon processing is on the same order of magnitude as that reported by Abbasi et al. when comparing CNT alignment derived from simple compression molding versus microinjection compression molding. Furthermore, ratios of $(ID/IG)_{\parallel}$ in unstrained and prestrained composites were 1.35 and 1.32, respectively, suggesting that the graphitic structure of CNTs has not been damaged upon straining.[40]

3.2. In Situ Temperature-Dependent NEXAFS Spectra.

Spectra acquired at increasing temperature registered increased emissions from C═C π^* and decreased emissions from C−H σ^*, C═O π^*, and C−O σ^* for all samples (Figure 6). In all cases, C−C σ^* emissions experienced small variations with temperature. Every material in the system (CNT, Phycol, and EVA) contributes to C−C σ^*. The actual C−C σ^* bonds are at many large angles to the average chain anisotropy, and chains are still flexible, so this orientational bias averages out. In addition, spherical symmetry from sigma bonds affords a higher tolerance toward conformational perturbations. This is not the

dx.doi.org/10.1021/jp409413k | J. Phys. Chem. C 2014, 118, 3733−3741

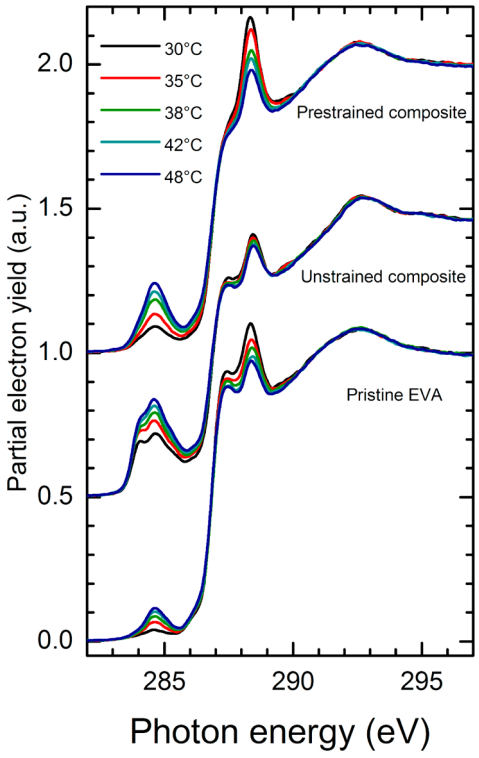

Figure 6. Carbon K-edge NEXAFS spectra of pristine EVA as well as unstrained and prestrained composites at various temperatures.

case for C═C π^*, which is highly directional and less accommodative of nonaxial deformations, often triggering concerns on pyramidalization.[43]

Decreased intensities of C−H and C═O groups in pristine EVA suggest rearrangement of polymeric chains. Figure 6 also shows increasing intensities at 284.5 eV with increasing temperature, possibly because of enhanced cross-linking of adsorbed contaminants on the surface of pristine EVA. Both σ^* C−H and π^* C═O intensities from the unstrained composite (Figure 6) decrease with increasing temperature, as was observed in pristine EVA, although to a much lesser extent. As CNTs are assumed to be randomly ordered if no strain is applied upon fabrication, an explanation for this scenario could revolve around CNTs acting as anchors for polymeric chains, preventing their rearrangement. In this scheme, CNTs would either restrict or cancel mobility within the polymeric system. Both C═C π^* intensities on the unstrained composites increase with temperature. As discussed earlier, the C═C π^* signal from pristine EVA is produced by a surfacial contamination layer, which increases with both irradiation time and temperature, as expected. The evolution of C═C π^* from both unstrained and strained EVA is attributed to intrinsic phenomena to the composites, as will be discussed in the next section.

Decreasing trends from C═O π^* intensities are enhanced on prestrained composites. In this case, the C−H σ^* emissions experience little variation with temperature. The C═C π^* intensities at 284.7 eV, contributed to mostly by CNT carbons and pyrenes from PyChol appended to graphitic wall, seem to increase with temperature with some correlation. In fact, pyrene groups at PyChol are likely to undergo the same deformations as CNT carbons. It is unclear if PyChol provides a homogeneous coverage of CNTs, and EVA molecules possibly bond to either pristine graphitic walls or PyChol-modified regions.

Relative intensities of C═C π^* and C═O π^* were computed to investigate trends of intensities with temperature. Figure 7 shows relative changes in the C═C π^* and C═O π^*

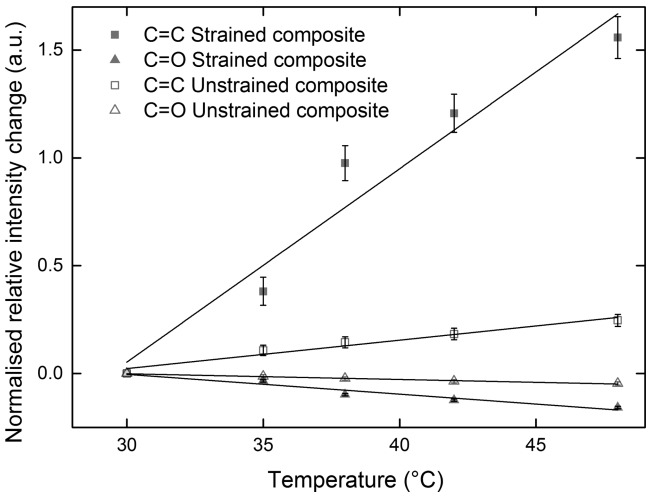

Figure 7. Relative change in the C═C and C═O emissions in composites with temperature.

emissions with respect to intensities at room temperature, calculated as $(I_i - I_{rt})/I_{rt}$, where the intensities are corrected for the surficial C═C π^* contamination contribution observed in pristine EVA. Trends are fairly linear. It is observed that trends of intensity variation (T_v) from strained composites are coupled, described by eq 1, by a factor of 10 ($x_{strained} = 10$). Furthermore, unstrained composites show weaker coupling by a factor of 5 ($x_{unstrained} = 5$). The implications of this result will be discussed in the next section because both chemical groups could be involved in temperature-driven dynamic effects on EVA composites.

$$T_{v(C=C)} = -xT_{v(C=O)} \quad (1)$$

In addition, the prestrained composite shows a greater sensitivity to temperature ($y_{C=C} = 7$ and $y_{C=O} = 4$ in eq 2), which is consistent with prior CNT alignment/actuation assumptions.[12,17] Results of these relations are summarized in Table 1.

$$T_{v(prestrained)} = yT_{v(unstrained)} \quad (2)$$

Indeed, prestraining is expected to align both CNTs and polymeric chains uniaxially with the purpose of enhancing actuation. Prestraining above 10% favors contraction along the straining axis;[12] this has been confirmed in EVA|MWCNTs composites.[26] Thermal conductivity is expected to increase with aligned CNTs, as they can provide more direct conductivity pathways across the entire composite thickness.[44] Increased thermal conductivity on the overall system could enhance the response. However, aligned CNT and polymeric chains could also present a different response to phonon coupling.

3.3. Conformational Model: Effects of Temperature on Molecular Orientation. A number of scenarios could occur that would lead to the trends shown in Figure 7. Decreasing intensities of 1s → $\pi^*_{C=O}$ could be explained as conformational changes in polymeric chains. Published work[35,45] has reported on molecular orientation as a function

dx.doi.org/10.1021/jp409413k | J. Phys. Chem. C 2014, 118, 3733−3741

Table 1. Fits and Ratios Derived from Temperature-Based Intensity Trends

	linear fits	ratios	
		C═C π^*/C═O π^*	strained/unstrained
C═C n* strained	$y = 0.089x - 2.64$	$T_{vC=C} = -10T_{v\ C=O}$	$T_{v\ C=C\ strained} = 7T_{v\ C=C\ unstrained}$
C═O n* strained	$y = -0.0091x + 0.27$		$T_{v\ C=O\ strained} = 4T_{v\ C=O\ unstrained}$
C═C n* unstrained	$y = 0.0131x - 0.37$	$T_{vC=C} = -5T_{v\ C=O}$	
C═O n* unstrained	$y = -0.0026x + 0.078$		

of temperature. To explore conformation further, NEXAFS spectra acquired at glancing (30°), magic (55°), and normal (90°) incident angles, both at room temperature and at 48 °C, were compared (Figure 8). Spectra acquired at room

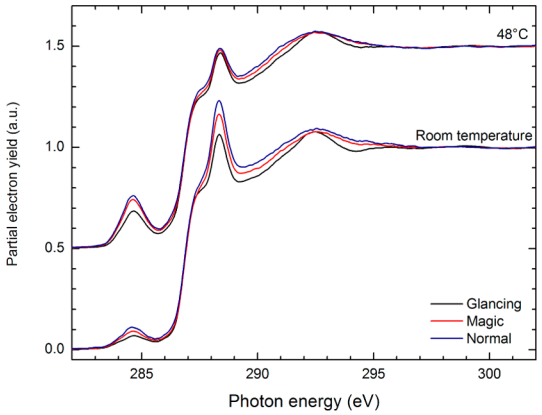

Figure 8. Angular dependence of prestrained EVA/0.7% CNT nanocomposite at room temperature and 48 °C.

temperature show a slight variation with incidence angle in both the C═C and C═O π^* emissions. Although the variation is small, it suggests that prestraining the sample results in some preferred orientation of CNTs (C═C π^* 284.7 eV emission) but more significantly of the polymer chains (288.4 eV emission corresponding to the 1s → $\pi^*_{C=O}$ transitions).

The angular dependence associated with the 288.4 eV emission is no longer apparent in spectra recorded at 48 °C, suggesting that C═O groups no longer have a preferred orientation. The 284.7 eV emission attributed to the 1s → $\pi^*_{C=C}$ transitions still shows an angular dependence. This effect could be explained by CNTs experiencing torsional perturbations with increasing temperature[12,15] while maintaining their overall uniaxial alignment. Polymer chains are likely to be wrapping around CNTs through noncovalent CH−π interactions,[46,47] resulting in C═O groups from EVA aligned at a preferred orientation with respect to the polymer backbone (Figure 9). Torsional straining on CNTs could therefore break the uniform orientation of C═O groups, as proposed in the model depicted in Figure 9. The lack of communication between adjacent PyChol molecules coating the outside wall of the MWCNT has important consequences. It inhibits the propagation of a perturbation from the underlying CNT through the pyrene lattice in PyChol. In this model, an isotropic distribution of C═O for PyChol follows, resulting in their omittance from both the discussion of thermal effects as well as the schematic of Figure 9.

A torsional deformation of carbon nanotubes could stretch bonds, leading to distortion of the π systems and making them less stable. Indeed, increased CNT diameters have been previously proposed as a result of increased bond lengths,

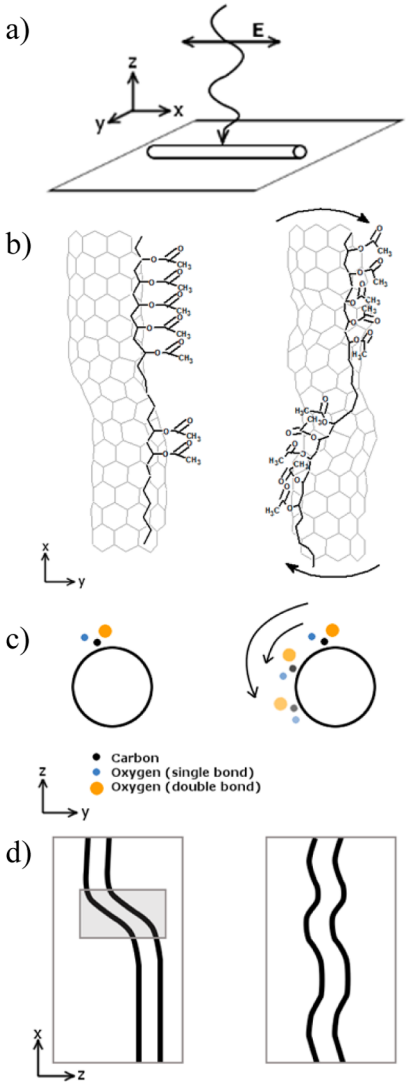

Figure 9. Beam travels along z axis with electric field vector along x axis (a). Proposed configuration of (left) strained EVA chain along a CNT side view (b) and top view (c) where the C═O bonds have a preferred orientation. Upon CNT torsion (right), C═O groups show an angular distribution. PyChol molecules have been omitted for simplicity. Cross-sectional view of CNT conformational changes upon actuation (d).

leading to more populated antibonding states,[48] and defective regions, as seen in Figure 4, could be especially prone to local twisting and bending.[49] In addition, suitability of CNTs to buckle and twist upon temperature and mechanical deformation opens the door to a number of conformational possibilities conducive to an increase in C═C emissions.[50]

Indeed, torsional responses of CNTs to stimuli is a recurrent topic in the literature of actuators, with Baughman and coworkers having recently proposed torsional CNTs toward

dx.doi.org/10.1021/jp409413k | J. Phys. Chem. C 2014, 118, 3733−3741

artificial muscles.[51,52] As Vaia had previously summarized,[19] CNT buckling is necessary to explain contractions of up to 15% (beyond reported strains in CNTs of 1 to 2%). How buckling would actually develop is still uncertain. Both a direct response from defective CNTs (responding in an inhomogeneous fashion to light) and inhomogeneity of local strain within the surrounding matrix have been proposed. In the second scenario, the prestrained polymeric chains would absorb thermal energy effectively supplied by CNTs, and they would contract, returning to a relaxed state. The mechanisms prone to yielding a response directly from the CNTs, as proposed in the first scenario, are still unclear.

The model in Figure 9 proposes a CNT upon straining with a preferential uniaxial configuration and with C═O groups in EVA also at a preferred orientation in the *xy* plane (Figure 9a,b), consistent with the early argument. However, synthesis and mechanical prestrain have not fully aligned the CNT either on the *xy* plane (as seen by the presence of kinks and bends) or on the *xz* plane (Figure 9d, left). In this configuration, π systems in the highlighted rectangular region (Figure 9d, left) would not be accessible to the beam and therefore would not contribute to the 1s → $\pi^*_{C=C}$ intensity.

Upon increased temperature, CNTs could experience additional torsion and buckling[50] that could result in increased uniaxial symmetry (Figure 9d, right), where a higher density of π systems are accessible to the beam and therefore contribute to the registered 1s → $\pi^*_{C=C}$ intensity. This effect could be promoting the observed increase in C═C emission intensity, as more transitions to $\pi^*_{C=C}$ are now accessible to the beam.

Intensity variations in 1s → $\pi^*_{C=C}$ and 1s → $\pi^*_{C=O}$ possibly result from conformational effects. Because CNTs and polymer chains are likely to be connected through CH−π interactions other than those remaining intact upon conformation (through the examined temperature range), it is not surprising that both emissions are indeed related. The implications of a 10-fold correlation in strained composites, however, are unclear, as a correlation between two geometrical conformations involving C═C and C═O bonds would need to be established. Clarification on the chemical origin of the observed 1s → $\pi^*_{C=O}$ signal is important to visualize a realistic actuation model. PyChol molecules are latched to CNTs by noncovalent $\pi-\pi$ interactions, as discussed earlier. Phenyl groups act as a coating layer to CNTs whose elements are not interconnected. The C═O group is bonded directly to the phenyls; therefore, because of the reduced size of phenyls and their lack of connectivity, any conformational movement of CNTs is not going to translate into a correlated conformation of the C═O groups. Variations of π^* C═O will be anisotropic, and their evolution with temperature would not correlate with π^* C═C, as seen in the NEXAFS spectra. The lack of connectivity between adjacent phenyl groups, as discussed above, ultimately renders the C═O groups in PyChol inefficient to flag conformation of CNTs and does not contribute significantly to the observed variation in the 1s → $\pi^*_{C=O}$ signal. It is worth highlighting that MWCNT in the PDMS composite did not use compatibilizers to disperse CNTs, yet bimodal photoactuation was reported.[11]

Moreover, CNT torsion and expansion effects have been proposed as key mechanisms behind mechanical actuation,[12,53] and our findings are consistent with those models. Mechanical actuation mechanisms were tentatively modeled first as rigid nanotubes suffering orientational order imposed by uniaxially applied strain.[12] More recently, smart behavior in hydrated media is seemingly related to polarization effects.[53] This scheme involved polarization at the polymer/CNT interface because of excitation of CNTs by incident light. Resulting electric fields could then promote migration of hydrogen ions and water molecules toward polymer/filler interfaces as well as distortion of the π systems in CNTs, resulting in mechanical bending.

The question certainly arises pertaining the nature of external stimulus on responses down to the molecular level. Are thermal and optical stimulation producing the same molecular dynamics? Actuation studies at the macroscopic level seem to suggest that all electrical, optical, and thermal external stimuli yield an internally induced thermal actuation.[54] The basis for this phenomenology is founded on the suitability of CNTs to modify thermally their surrounding environments (i.e., a thermal perturbation is induced locally on surrounding polymer/elastomer either by melting[19] or by the contraction/relaxation of the polymeric chains, depending on prestraining history).[12,17] Further supporting this hypothesis, Hu et al.[54] recently emphasized the importance of internal thermal actuation in polymer nanocomposites, where CNTs are believed to function as nanoantennas, converting external stimulus to strategically localized thermal perturbations in the composite. The availability of simultaneous cooling and heating capabilities for in situ NEXAFS could offer further insight into the nature of these thermal effects.

If CNTs indeed convert external light into localized heat other than actuation kinetics, then dynamic effects observed by NEXAFS during external heating are likely to be comparable to those during external heating reported by Czanikova et al.[17] in which a macroscopic mechanical actuation was observed. This discussion suggests that CNT−phonon coupling could be inducing both CNT torsional effects and polymer conformation at the molecular level. How this phenomenology would produce a macroscopic response is in need of further investigation.

4. CONCLUSIONS

The thermal-induced effects promoting molecular conformation on EVA | CNT composites were studied by NEXAFS. Our results show inverse variations in intensity between the emissions at 284.8 and 288.5 eV with temperature, associated with the 1s → $\pi^*_{C=C}$ and 1s → $\pi^*_{C=O}$ transitions. Intensities in prestrained composites are linearly correlated by a factor of 10 across the investigated temperature range. These findings suggest strong conformational coupling between C═C from CNTs and C═O from EVA, possibly involving CNT torsional effects. Both a direct response from defective CNTs (responding in an inhomogeneous fashion to light) and inhomogeneity of local strain within the surrounding matrix have been proposed. The observed dynamics at the molecular level could contribute to the macroscopically observed thermal actuation.

■ AUTHOR INFORMATION

Notes

The authors declare no competing financial interest.

■ ACKNOWLEDGMENTS

We kindly acknowledge Professor Eugene Terentjev at Cambridge University and Conan Weiland at Synchrotron Research Inc. for insightful discussions. Research was carried

out in part at the National Synchrotron Light Source at Brookhaven National Laboratory, which is supported by the U.S. Department of Energy under contract number DE-AC02-98CH10886. This project was partially founded by FP7VEGA 2/0149/14 and NMP 22896 and by grants from the National Center for Research Resources (5 G12RR013646-12) and the National Institute on Minority Health and Health Disparities (G12MD007591) from the National Institutes of Health. We acknowledge the NSF for support with grants DMR-1103730, Alloys at the Nanoscale: The Case of Nanoparticles Second Phase and PREM: NSF PREM grant DMR-0934218.

REFERENCES

(1) Ebron, V. H.; Yang, Z.; Seyer, D. J.; Kozlov, M. E.; Oh, J.; Xie, H.; Razal, J.; Hall, L. J.; Ferraris, J. P.; MacDiarmid, A. G.; et al. Fuel-Powered Artificial Muscles. *Science* **2006**, *311*, 1580−1583.
(2) Behl, M.; Razzaq, M. Y.; Lendlein, A. Multifunctional Shape-Memory Polymers. *Adv. Mater.* **2010**, *22*, 3388−3410.
(3) Ionov, L. Actively-Moving Materials Based on Stimuli-Responsive Polymers. *J. Mater. Chem.* **2010**, *20*, 3382−3390.
(4) Ikeda, T.; Ube, T. Photomobile Polymer Materials: From Nano to Macro. *Mater. Today* **2011**, *14*, 480−487.
(5) Iijima, S. Helical Microtubules of Graphitic Carbon. *Nature* **1991**, *354*, 56−58.
(6) Baughman, R. H.; Cui, C. X.; Zakhidov, A. A.; Iqbal, Z.; Barisci, J. N. Carbon Nanotube Actuators. *Science* **1999**, *284*, 1340−1344.
(7) Moniruzzaman, M.; Winey, K. I. Polymer Nanocomposites Containing Carbon Nanotubes. *Macromolecules* **2006**, *39*, 5194−5205.
(8) Ohm, C.; Brehmer, M.; Zentel, R. Liquid Crystalline Elastomers as Actuators and Sensors. *Adv. Mater.* **2010**, *22*, 3366−3387.
(9) Yan, Z.; Ji, X.; Wu, W.; Wei, J.; Yu, Y. Light-Switchable Behavior of a Microarray of Azobenzene Liquid Crystal Polymer Induced by Photodeformation. *Macromol. Rapid Commun.* **2012**, *33*, 1362−1367.
(10) Sánchez-Ferrer, A.; Merekalov, A.; Finkelmann, H. Opto-Mechanical Effect in Photoactive Nematic Side-Chain Liquid-Crystalline Elastomers. *Macromol. Rapid Commun.* **2011**, *32*, 671−678.
(11) Ahir, S. V.; Squires, A. M.; Tajbakhsh, A. R.; Terentjev, E. M. Infrared Actuation in Aligned Polymer-Nanotube Composites. *Phys. Rev. B* **2006**, *73*, 085420−12.
(12) Ahir, S. V.; Terentjev, E. M. Fast Relaxation of Carbon Nanotubes in Polymer Composite Actuators. *Phys. Rev. Lett.* **2006**, *96*, 133902−133904.
(13) Loomis, J.; King, B.; Burkhead, T.; Xu, P.; Bessler, N.; Terentjev, E.; Panchapakesan, B. Graphene-Nanoplatelet-Based Photomechanical Actuators. *Nanotechnology* **2012**, *23*, 045501-1−045501-10.
(14) Sellinger, A. T.; Wang, D. H.; Tan, L.; Vaia, R. A. Electrothermal Polymer Nanocomposite Actuators. *Adv. Mater.* **2010**, *22*, 3430−3435.
(15) Ahir, S. V.; Terentjev, E. M. Photomechanical Actuation in Polymer-Nanotube Composites. *Nat. Mater.* **2005**, *4*, 491−495.
(16) Campo, E. M.; Roig, J.; Roeder, B.; Wenn, D.; Mamojka, B.; Omastová, M.; Terentjev, E. M.; Esteve, J. Nano-Opto Mechanical Systems (NOMS) as a Proposal for Tactile Displays. *Proc. SPIE* **2011**, *8107*, 81070H-1−81070H-10.
(17) Czaniková, K.; Krupa, I.; Iláíková, M.; Kasák, P.; Chorvár, D.; Valentin, M.; Šlouf, M.; Mosnáček, J.; Mičušík, M.; Omastová, M. Photo-Actuating Materials Based on Elastomers and Modified Carbon Nanotubes. *J. Nanophotonics* **2011**, 063522_1−14.
(18) Ahir, S. V.; Huang, Y. Y.; Terentjev, E. M. Polymers with Aligned Carbon Nanotubes: Active Composite Materials. *Polymer* **2008**, *49*, 3841−3854.
(19) Vaia, R. Nanocomposites: Remote-Controlled Actuators. *Nat. Mater.* **2005**, *4*, 429−430.
(20) Li, J.; Rodgers, W. R.; Xie, T. Semi-Crystalline Two-Way Shape Memory Elastomer. *Polymer* **2011**, *52*, 5320−5325.
(21) Nativ-Roth, E.; Shvartzman-Cohen, R.; Bounioux, C.; Florent, M.; Zhang, D.; Szleifer, I.; Yerushalmi-Rozen, R. Physical Adsorption of Block Copolymers to SWNT and MWNT: A Nonwrapping Mechanism. *Macromolecules* **2007**, *40*, 3676−3685.
(22) Tung, W.; Bird, V.; Composto, R. J.; Clarke, N.; Winey, K. I. Polymer Chain Conformations in CNT/PS Nanocomposites from Small Angle Neutron Scattering. *Macromolecules* **2013**, *46*, 5345−5354.
(23) Laird, E. D.; Li, C. Y. Structure and Morphology Control in Crystalline Polymer−Carbon Nanotube Nanocomposites. *Macromolecules* **2013**, *46*, 2877−2891.
(24) Liu, Y.; Russell, T. P.; Samant, M. G.; Stöhr, J.; Brown, H. R.; Cossy-Favre, A.; Diaz, J. Surface Relaxations in Polymers. *Macromolecules* **1997**, *30*, 7768−7771.
(25) Pattison, L. R.; Hexemer, A.; Kramer, E. J.; Krishnan, S.; Petroff, P. M.; Fischer, D. A. Probing the Ordering of Semiconducting Fluorene-Thiophene Copolymer Surfaces on Rubbed Polyimide Substrates by near-Edge X-Ray Absorption Fine Structure. *Macromolecules* **2006**, *39*, 2225−2231.
(26) Czaniková, K.; Torras, N.; Esteve, J.; Krupa, I.; Kasák, P.; Pavlova, E.; Račko, D.; Chodák, I.; Omastová, M. Nanocomposite Photoactuators Based on an Ethylene Vinyl Acetate Copolymer Filled with Carbon Nanotubes. *Sens. Actuators, B* **2013**, *186*, 701−710.
(27) Fleming, L.; Ulrich, M. D.; Efimenko, K.; Genzer, J.; Chan, A. S. Y.; Madey, T. E.; Oh, S.-J.; Zhou, O.; Rowe, J. E. Near-Edge Absorption Fine Structure and UV Photoemission Spectroscopy Studies of Aligned Single-Walled Carbon Nanotubes on Si (100) Substrates. *J. Vac. Sci. Technol., B: Microelectron. Nanometer Struct.* **2004**, *22*, 2000−2004.
(28) Banerjee, S.; Hemraj-Benny, T.; Balasubramanian, M.; Fischer, D.; Misewich, J. A.; Wong, S. S. Surface Chemistry and Structure of Purified, Ozonized, Multiwalled Carbon Nanotubes Probed by NEXAFS and Vibrational Spectroscopies. *ChemPhysChem* **2004**, *5*, 1416−1422.
(29) Pozdnyakov, A. O.; Brzhezinskaya, M. M.; Vinogradov, A. S.; Friedrich, K. NEXAFS Spectra of Polymer-Nanocarbon Composites. *Fullerenes, Nanotubes, Carbon Nanostruct.* **2008**, *16*, 471−474.
(30) Martín, Z.; Jiménez, I.; Ángeles Gómez, M.; Ade, H.; Kilcoyne, D. A. Interfacial Interactions in Pp/Mmt/Sebs Nanocomposites. *Macromolecules* **2010**, *43*, 448−453.
(31) Collins, B. A.; Li, Z.; McNeill, C. R.; Ade, H. Fullerene-Dependent Miscibility in the Silole-Containing Copolymer PSBTBT-08. *Macromolecules* **2011**, *44*, 9747−9751.
(32) Komornicki, J.; Bourrel, M.; Marin, G.; Brogly, M. Thermal and Visco-Elastic Properties of EVA-Based Hot-Melt Adhesives: Relationship to Peel Behaviour. *J. Adhes. Sci. Technol.* **1992**, *6*, 293−305.
(33) Stöhr, J. *NEXAFS Spectroscopy*; Springer: New York, 2003.
(34) DeLongchamp, D. M.; Kline, R. J.; Fischer, D. A.; Richter, L. J.; Toney, M. F. Molecular Characterization of Organic Electronic Films. *Adv. Mater.* **2010**, *23*, 319−337.
(35) Genzer, J.; Sivaniah, E.; Kramer, E. J.; Wang, J.; Korner, H.; Char, K.; Ober, C. K.; DeKoven, B. M.; Bubeck, R. A.; Fischer, D. A.; et al. Temperature Dependence of Molecular Orientation on the Surfaces of Semifluorinated Polymer Thin Films. *Langmuir* **2000**, *16*, 1993−1997.
(36) Ravel, B.; Newville, M. Athena, Artemis, and Hephaestus: Data Analysis for X-Ray Absorption Spectroscopy Using Ifeffit. *J. Synchrotron Radiat.* **2005**, *12*, 537−541.
(37) Hemraj-Benny, T.; Banerjee, S.; Sambasivan, S.; Balasubramanian, M.; Fischer, D.; Eres, G.; Puretzky, A. A.; Geohegan, D. B.; Lowndes, D. H.; Han, W.; et al. Near-Edge X-Ray Absorption Fine Structure Spectroscopy as a Tool for Investigating Nanomaterials. *Small* **2006**, *2*, 26−35.
(38) Hirsch, A. Functionalization of Single-Walled Carbon Nanotubes. *Angew. Chem., Int. Ed.* **2002**, *41*, 1853−1859.
(39) Koh, A. L.; Gidcumb, E.; Zhou, O.; Sinclair, R. Observations of Carbon Nanotube Oxidation in an Aberration-Corrected Environmental Transmission Electron Microscope. *ACS Nano* **2013**, *7*, 2566−2572.
(40) Abbasi, S.; Carreau, P. J.; Derdouri, A. Flow Induced Orientation of Multiwalled Carbon Nanotubes in Polycarbonate Nanocomposites: Rheology, Conductivity and Mechanical Properties. *Polymer* **2010**, *51*, 922−935.

(41) Dresselhaus, M. S.; Jorio, A.; Hofmann, M.; Dresselhaus, G.; Saito, R. Perspectives on Carbon Nanotubes and Graphene Raman Spectroscopy. *Nano Lett.* **2010**, *10*, 751−758.
(42) Shimoyama, M.; Maeda, H.; Matsukawa, K.; Inoue, H.; Ninomiya, T.; Ozaki, Y. Discrimination of Ethylene/Vinyl Acetate Copolymers with Different Composition and Prediction of the Vinyl Acetate Content in the Copolymers Using Fourier-Transform Raman Spectroscopy and Multivariate Data Analysis. *Vib. Spectrosc.* **1997**, *14*, 253−259.
(43) Banerjee, S.; Hemraj Benny, T.; Wong, S. S. Covalent Surface Chemistry of Single-Walled Carbon Nanotubes. *Adv. Mater.* **2005**, *17*, 17−29.
(44) Marconnet, A. M.; Yamamoto, N.; Panzer, M. A.; Wardle, L. B.; Goodson, K. E. Thermal Conduction in Aligned Carbon Nanotube−Polymer Nanocomposites with High Packing Density. *ACS Nano* **2011**, *5*, 4818−4821.
(45) Yamamoto, Y.; Mitsumoto, R.; Araki, T.; Ouchi, Y.; Ishii, H.; Seki, K.; Ueno, N.; Takanishi, Y. NEXAFS Studies on the Surface Structure of Liquid N-C50H102 (Pentacontane). *J. Phys.* **1997**, *IV*, C2709−C2710.
(46) Beigbeder, A.; Linares, M.; Devalckenaere, M.; Degée, P.; Claes, M.; Beljonne, D.; Lazzaroni, R.; Dubois, P. CH-π Interactions as the Driving Force for Silicone-Based Nanocomposites with Exceptional Properties. *Adv. Mater.* **2008**, *20*, 1003−1007.
(47) Teh, S. L.; Linton, D.; Dadmun, M. D. Controlling Non-Covalent Interactions to Modulate the Dispersion of Fullerenes in Polymer Nanocomposites. *Macromolecules* **2011**, *44*, 7737−7745.
(48) Sun, G.; Kürti, J.; Kertesz, M.; Baughman, R. H. Dimensional Changes as a Function of Charge Injection in Single-Walled Carbon Nanotubes. *J. Am. Chem. Soc.* **2002**, *124*, 15076−15080.
(49) Gartstein, Y. N.; Zakhidov, A. A.; Baughman, R. H. Mechanical and Electromechanical Coupling in Carbon Nanotube Distortions. *Phys. Rev. B* **2003**, *68*, 115415−115426.
(50) Zhang, Y. Y.; Wang, C. M.; Tan, V. B. C. Buckling of Carbon Nanotubes at High Temperatures. *Nanotechnology* **2009**, *20*, 215702−215710.
(51) Foroughi, J.; Spinks, G. M.; Wallace, G. G.; Oh, J.; Kozlov, M. E.; Fang, S.; Mirfakhrai, T.; Madden, J. D. W.; Shin, M. K.; Kim, S. J.; et al. Torsional Carbon Nanotube Artificial Muscles. *Science* **2011**, *334*, 494−497.
(52) Lima, M. D.; Li, N.; Jung de Andrade, M.; Fang, S.; Oh, J.; Spinks, G. M.; Kozlov, M. E.; Haines, C. S.; Suh, D.; Foroughi, J.; et al. Electrically, Chemically, and Photonically Powered Torsional and Tensile Actuation of Hybrid Carbon Nanotube Yarn Muscles. *Science* **2012**, *338*, 928−932.
(53) Viola, E. A.; Levitsky, I. A.; Euler, W. B. Kinetics of Photoactuation in Single Wall Carbon Nanotube−Nafion Bilayer Composite. *J. Phys. Chem. C* **2010**, *114*, 20258−20266.
(54) Hu, Y.; Chen, W. Externally Induced Thermal Actuation of Polymer Nanocomposites. *Macromol. Chem. Phys.* **2011**, *212*, 992−998.